Engineered neutrophil-derived exosome-like vesicles for targeted cancer therapy

Zhang, Jiahui

2022-01

Zhang , J , Ji , C , Zhang , H , Shi , H , Mao , F , Qian , H , Xu , W , Wang , D , Pan , J , Fang , X , Santos , H A & Zhang , X 2022 , ' Engineered neutrophil-derived exosome-like vesicles for targeted cancer therapy ' , Science Advances , vol. 8 , no. 2 , 8207 . https://doi.org/10.1126/sciadv.abj8207

http://hdl.handle.net/10138/341389
https://doi.org/10.1126/sciadv.abj8207

CANCER

Engineered neutrophil-derived exosome-like vesicles for targeted cancer therapy

Jiahui Zhang[1]†, Cheng Ji[1]†, Hongbo Zhang[2,3]†, Hui Shi[1], Fei Mao[1], Hui Qian[1], Wenrong Xu[1], Dongqing Wang[4], Jianming Pan[5], Xinjian Fang[6]*, Hélder A. Santos[7,8]*, Xu Zhang[1]*

Neutrophils are the most abundant innate immune cells in human circulation; however, their derived exosomes have been rarely studied for tumor treatment. Here, we reported that exosomes from neutrophils (N-Ex) induce tumor cell apoptosis by delivering cytotoxic proteins and activating caspase signaling pathway. In addition, we decorated N-Ex with superparamagnetic iron oxide nanoparticles (SPIONs) to achieve higher tumor-targeting therapeutic effect. We further fabricated exosome-like nanovesicles from neutrophils (NNVs) at high yield. Compared with liposome-loaded doxorubicin (DOX) and natural NNVs, DOX-loaded NNVs show an improved inhibition of tumor cell proliferation. Moreover, DOX-loaded, SPION-decorated NNVs selectively accumulate at the tumor sites under an external magnetic field, effectively restraining tumor growth and extensively prolonging the survival rate in mice. Overall, a simple and effective method to engineer N-Ex and NNVs at clinical applicable scale was developed, which enables the efficient and safe drug delivery for targeted and combined tumor therapy.

INTRODUCTION

Neutrophils are the most abundant innate immune cells in human circulation and act as the first line of defense against infection. Previous studies demonstrate that neutrophils can eliminate malignant tumor cells by direct cytotoxicity to tumor cells, antibody-dependent cytotoxic activity, and recruitment of other antitumor effector cells (*1*). Neutrophils can release cytotoxic substrates such as reactive oxygen species and hydrogen peroxide (H_2O_2) to mediate tumor cell killing (*2*). In addition, neutrophils are capable of activating Fas/FasL (Fas ligand) apoptosis signaling pathway and directly promoting tumor cell death. Neutrophils can also produce a wide spectrum of factors to inhibit tumor cell proliferation (*2*). Therefore, better understanding of the antitumor activity of neutrophils will provide a previously unknown approach for cancer therapy.

Exosomes are a class of extracellular vesicles (EVs) that play important roles in intercellular communication (*3*). Recently, exosomes from immune cells have shown potent antitumor activity similar to their producing cells. For instance, dendritic cell–derived exosomes promote tumor cell apoptosis via TNF (tumor necrosis factor) superfamily ligands (*4*). In addition, natural killer (NK) cell–derived exosomes exert cytotoxic effects on tumor cells by delivering functional NK proteins, namely, FasL and perforin (*5*–*8*). Moreover, exosomes derived from γδ2-T cells contain death-inducing ligands [FasL and TRAIL (TNF related apoptosis inducing ligand)], which target and efficiently kill Epstein-Barr virus–associated tumor cells (*9*). Previous studies have used neutrophil-derived EVs to treat arthritis and sepsis (*10*, *11*). However, the role of neutrophil-derived exosomes (N-Ex) in cancer therapy has not been fully explored, mainly because of the short half-life of neutrophil and low yield of N-Ex.

Chemotherapy is commonly used in the clinic, but most chemotherapeutic drugs lack tumor-targeting ability and have toxic effects on normal cells. Increasing evidence suggests that exosomes can be used as a new tool for delivering chemotherapeutic agents because of several advantages (*12*–*14*). For instance, exosomes are intrinsically biocompatible, biodegradable, and low toxic. In addition, exosomes can escape from clearance by the host immune system and pass through physiological barriers. Moreover, exosomes inherit natural targeting properties from their producing cells and accumulate at local and metastatic tumor sites after systemic infusion (*13*). For instance, exosomes derived from M1-polarized macrophages have been used to deliver paclitaxel, which showed a higher antitumor activity than free drug in mice (*6*). More recently, through extrusion, exosome-like nanovesicles (NVs) have been produced at high yield and emerged as a highly efficient exosome-like drug delivery system (*15*–*20*). Whether NVs from neutrophils (NNVs) could be used for cancer treatment remains unknown.

To this end, we determined the roles of natural N-Ex and exosome-like NNVs in cancer therapy. We first demonstrated that N-Ex exerted notable antitumor effect by activating the apoptosis signaling pathway. We then decorated N-Ex with superparamagnetic iron oxide nanoparticles (SPIONs) for targeted cancer therapy. Furthermore, we prepared NNVs loaded with doxorubicin (NNV-DOX) by an extrusion method and decorated them with SPION (SPION-NNV-DOX) to achieve a dual-targeting property and combined antitumor response. Our study suggests that the engineered SPION-NNVs are very powerful in targeted drug delivery and cancer therapy, and it can be produced at high yield for clinical translation.

RESULTS

Isolation, characterization, and uptake of N-Ex

To produce N-Ex, we isolated neutrophils from the peripheral blood of healthy donors and cultured them in exosome-free medium for

[1]Jiangsu Key Laboratory of Medical Science and Laboratory Medicine, School of Medicine, Jiangsu University, 212013 Zhenjiang, China. [2]Pharmaceutical Sciences Laboratory, Åbo Akademi University, 20520 Turku, Finland. [3]Turku Biosciences Center, University of Turku and Åbo Akademi University, 20520 Turku, Finland. [4]Department of Radiology, Affiliated Hospital of Jiangsu University, Jiangsu University, 212001 Zhenjiang, China. [5]School of Chemistry and Chemical Engineering, Jiangsu University, 212013 Zhenjiang, China. [6]Department of Oncology, Lianyungang Hospital Affiliated to Jiangsu University, Lianyungang, Jiangsu 222000, China. [7]Department of Biomedical Engineering, University Medical Center Groningen/University of Groningen, W.J. Kolff Institute for Biomedical Engineering and Materials Science, Ant. Deusinglaan 1, 9713 AV Groningen, Netherlands. [8]Drug Research Program, Division of Pharmaceutical Chemistry and Technology, Faculty of Pharmacy, University of Helsinki, FI-00014 Helsinki, Finland.
*Corresponding author. Email: xuzhang@ujs.edu.cn (X.Z.); h.a.santos@umcg.nl (H.A.S.); lygfxj@126.com (X.F.)
†These authors contributed equally to this work.

24 hours. N-Ex were isolated from the conditioned medium of neutrophils (N-CM) by ultracentrifugation and purified by density gradient centrifugation (Fig. 1A). In general, the protein content of N-Ex from 500 ml of culture supernatant of neutrophils was about 20 g/liter [as determined by bicinchoninic acid (BCA) protein assay]. The vesicular structure of N-Ex was measured by transmission electron microscopy (TEM; Fig. 1B). N-Ex displayed a cup-shaped morphology with a diameter of 30 to 150 nm. The atomic force microscopy (AFM) images of N-Ex showed a typical oval structure of exosomes and the pattern of N-Ex in three-dimensional imaging in an oblique view (Fig. 1, C and D). Moreover, the nanoparticle tracking analysis (NTA) results showed that N-Ex had an average diameter of 125 ± 10 nm and zeta potential of −26 ± 1 mV, which is consistent with TEM morphology (Fig. 1, E and F). The polydispersity index (PDI) of N-Ex was detected by dynamic light scattering (DLS) and showed a value lower than 0.3 (Fig. 1G). Further characterization by Western blot confirmed that N-Ex expressed exosomal markers CD9, CD63, CD81, and Alix, but not the endoplasmic reticulum (ER) marker calnexin (Fig. 1H). Therefore, these results suggest that exosomes were successfully isolated from human neutrophils. To determine whether N-Ex could be taken up by tumor cells, we labeled N-Ex with 1,1-dioctadecyl-3,3,3,3-tetramethylindotricarbocyaine iodide (DiR) fluorescent dye and incubated them with HGC27, SW480, and HepG2 cells for different times. The results of imaging flow cytometry and fluorescence confocal laser microscopy showed that N-Ex was efficiently internalized into tumor cells in a time-dependent manner (Fig. 1, I and J, and fig. S1).

N-Ex display tumor-suppressive activity both in vitro and in vivo

Next, we performed Cell Counting Kit-8 (CCK-8) assay to determine the effect of N-Ex on the proliferation of tumor cells (HGC27, SW480, and HepG2) and normal cells [GES-1, human umbilical vein endothelial cells (HUVEC), and human fibroblasts (HFL)]. We chose 40 μg/ml as the work dose because this concentration had stable and efficient effect on tumor cell inhibition (fig. S2, D to F). On the contrary, N-Ex had minimal effect on the proliferation of normal cells (fig. S2, A to C). Compared to the control group, the proliferation ability of HGC27 cells was significantly inhibited by incubation with N-Ex but not N-Ex–depleted CM (Fig. 2A). Similar effects of N-Ex were also observed in cell colony formation assays (figs. S3 and S4). Flow cytometry results showed that N-Ex induced significant apoptosis in tumor cells but not normal cells at 24 hours after treatment (Fig. 2, B and C, and figs. S5 and S6). In addition, JC-1 staining results showed that the mitochondrial membrane potential of tumor cells was notably elevated after N-Ex treatment (Fig. 2D and fig. S7). Then, HGC27 cells treated with N-Ex (40 μg/ml) for 24 hours were evaluated for the status of apoptosis signaling pathway proteins. Western blot results showed that N-Ex treatment increased the expression levels of cleaved caspase-3, cleaved caspase-7, cleaved

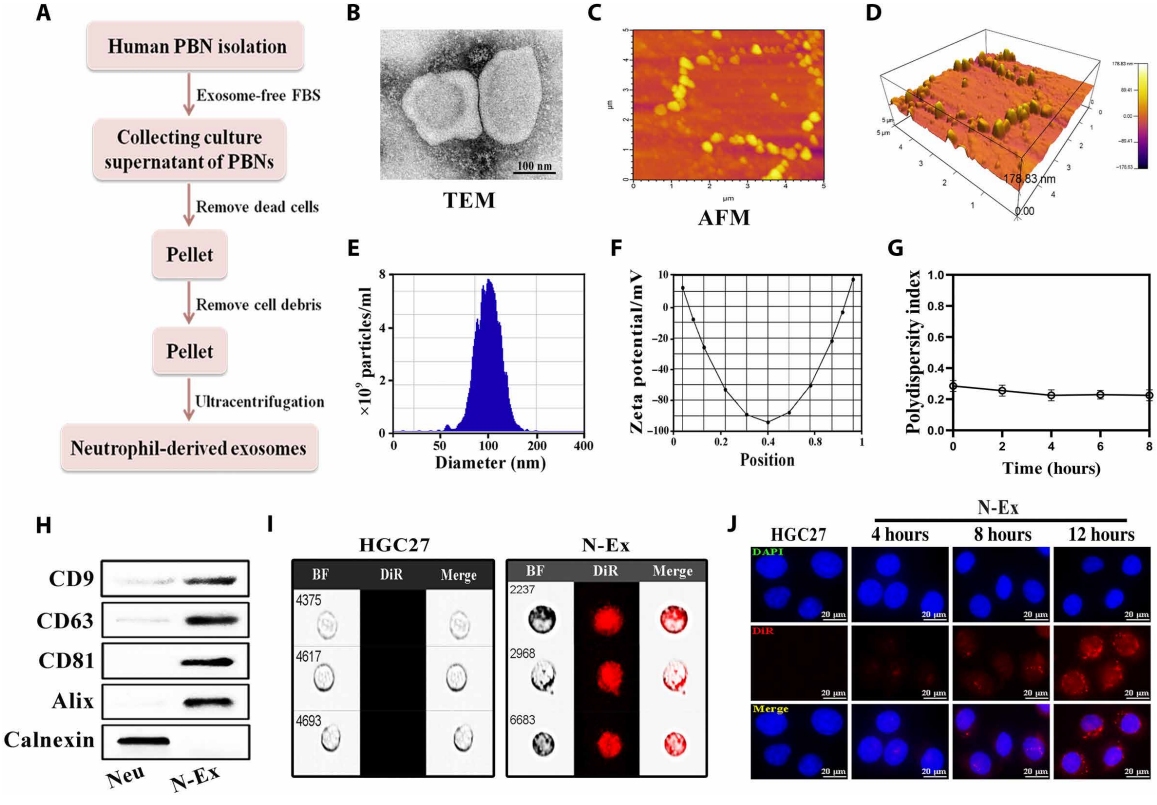

Fig. 1. Isolation, characterization, and cellular uptake of N-Ex. (**A**) Schematic diagram for the isolation of exosomes from human peripheral blood neutrophils (PBNs). (**B**) TEM images of N-Ex. Scale bar, 100 nm. (**C** and **D**) N-Ex morphology was determined by atomic force microscopy (AFM). (**E** and **F**) NTA of particle size (E) and zeta potential (F) of N-Ex. (**G**) The PDI of N-Ex was tested by DLS. (**H**) Western blot analyses of exosomal biomarkers (CD9, CD63, CD81, and Alix) and ER marker (calnexin) in N-Ex. Neutrophil (Neu) lysate was used as a control. (**I** and **J**) Internalization of DiR-labeled N-Ex by human gastric cancer cells (HGC27) was determined by imaging flow cytometry (I) and fluorescence confocal laser microscopy (J). Cell nuclei were counterstained with 4′,6-diamidino-2-phenylindole (DAPI). BF, bright field. Scale bars, 20 μm.

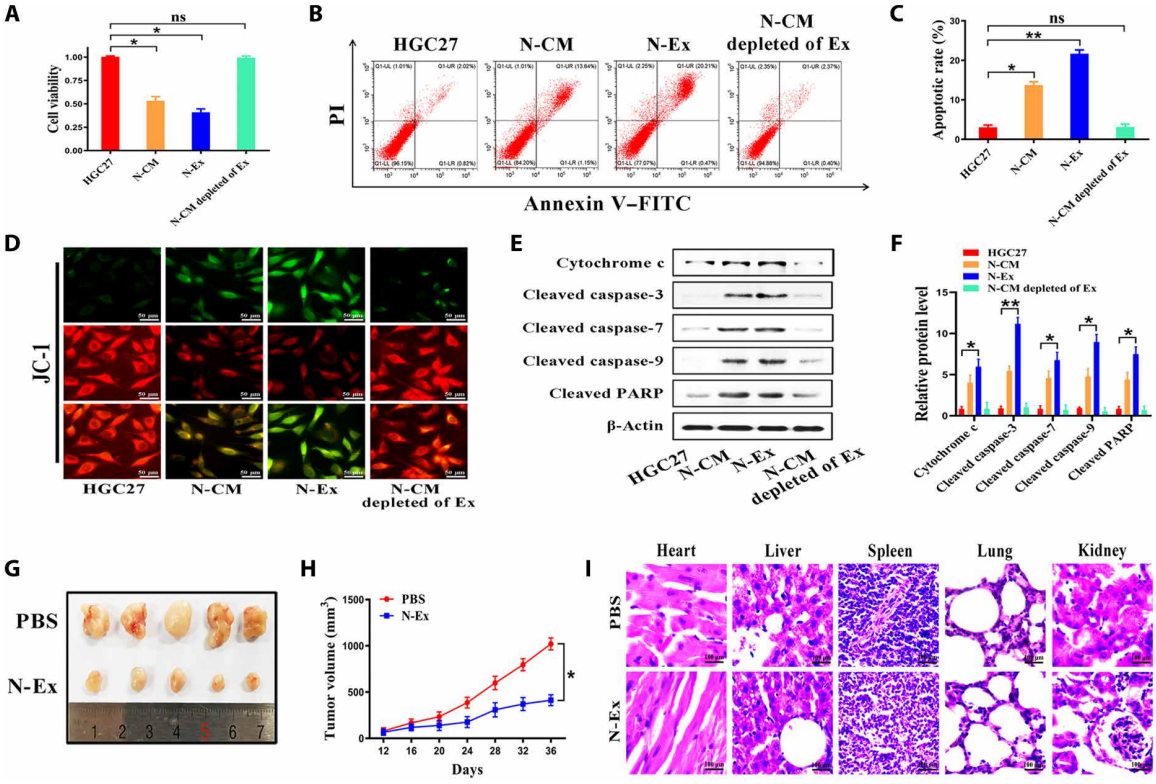

Fig. 2. N-Ex display tumor-suppressive activity both in vitro and in vivo. (**A**) CCK-8 assays for the cytotoxicity of CM, exosomes (40 μg/ml), and exosome-depleted CM from neutrophils on human gastric cancer cells (HGC27) at 24 hours after incubation. (**B** and **C**) Flow cytometry analyses of cell apoptosis in human gastric cancer cells (HGC27) treated with N-Ex (40 μg/ml) for 24 hours. PI, propidium iodide; FITC, fluorescein isothiocyanate. (**D**) Effects of N-Ex (40 μg/ml) on mitochondrial membrane potential were determined by JC-1 staining. Scale bars, 50 μm. (**E** and **F**) Western blot assays for the expression of proteins in apoptosis signaling pathway in HGC27 cells treated with N-Ex (40 μg/ml) for 24 hours. PARP, poly(adenosine diphosphate–ribose) polymerase. (**G**) Images of subcutaneous xenograft tumors in BALB/c nude mice ($n = 5$ per group) treated with PBS and N-Ex (5 mg/kg of body weight; 100 μl). (**H**) Tumor growth curves of BALB/c nude mice in PBS- and N-Ex–treated groups ($n = 5$ per group). (**I**) H&E staining of the heart, liver, spleen, lung, and kidney of mice as indicated. One-way analysis of variance (ANOVA) for multiple groups and Student's *t* test for paired two groups were applied for statistical analysis. Scale bars, 100 μm. ns, no significant change. *$P < 0.05$ and **$P < 0.01$.

caspase-9, cleaved poly(adenosine diphosphate–ribose) polymerase (PARP), and cytochrome c in HGC27 cells (Fig. 2, E and F). Similar changes were also observed in SW480 and HepG2 cells (fig. S8). Moreover, the results of Western blot indicated that FasL, granzyme A, granzyme B, and perforin were present in N-Ex (fig. S10), suggesting that these proteins may play an important role in promoting tumor cell apoptosis. We also compared the effects of N-Ex with that of peripheral blood mononuclear cell (PBMC)–derived exosomes (PBMCs-Ex; 40 μg/ml). CCK-8 results showed that N-Ex exhibited a higher inhibitory effect than PBMCs-Ex on HGC27 cell proliferation (fig. S9). Together, these results suggest that N-Ex inhibit tumor cell viability in vitro by activating apoptosis signaling pathway.

We then subcutaneously injected HGC27 cells into BALB/c nude mice and generated xenograft tumor models to evaluate the antitumor efficacy of N-Ex. When tumor size reached ~50 mm^3 ($n = 5$ per group), the mice were treated with N-Ex (5 mg/kg of body weight) via intravenous injection every 4 days for 7 cycles (fig. S11A). The major organs and tumors were collected at 3 days after the last injection (day 39). As shown in fig. S11 (B and C), the fluorescence signals of administrated N-Ex (labeled with DiR) were mainly accumulated in the liver and spleen, while a relatively weak fluorescence signal was observed in the tumors. In comparison with the phosphate-buffered saline (PBS) group, the N-Ex treatment group yielded a significant inhibition of tumor growth (Fig. 2G). The average tumor volume in mice treated with N-Ex stayed at <500 mm^3, whereas the body weight of mice did not significantly reduce (Fig. 2H and fig. S11D). We further detected the expression of apoptosis-related proteins in the tumors by Western blot analysis. We found that N-Ex treatment led to a significant promotion of cell apoptosis by activating the caspase signaling pathway in the tumors (fig. S11, E and F). In addition, Ki-67 and terminal deoxynucleotidyl transferase–mediated deoxyuridine triphosphate nick end labeling (TUNEL) staining results showed that the tumors from the N-Ex group displayed less Ki-67–positive (fig. S11, G and H) while more TUNEL-positive cells (fig. S11, I and J) than those from the PBS group, which further confirmed that N-Ex suppressed tumor growth by inducing apoptosis. The results of hematoxylin and eosin (H&E) staining showed that N-Ex treatment did not cause cell degeneration or necrosis in major organs (heart, liver, spleen, lung, and kidney), indicating that N-Ex had no overt systemic toxicity (Fig. 2I). Consistent with this result, the serum levels of indicators for liver [ALT (alanine aminotransferase) and (aspartate aminotransferase)], kidney [BUN (blood urea nitrogen) and CREA (creatinine)], and heart [CK (creatine Kinase), CK-MB (creatine kinase isoenzymes), LDH (lactate dehydrogenase), and α-HBDH (α-hydroxybutyrate dehydrogenase)] functions in N-Ex–treated mice were not significantly different with

that in PBS-treated mice (fig. S12). Furthermore, the cryosections of the liver and spleen showed stronger red fluorescence signals than that of tumors, indicating that DiR-labeled N-Ex were mainly retained in these organs (fig. S13). We also treated the mice (n = 5 per group) with N-Ex by intratumoral injection (5 mg/kg of body weight) and observed a stronger antitumor efficacy than intravenous injection (fig. S14). Together, these results suggest that N-Ex exerts an efficient and safe antitumor effect in vivo.

Preparation and characterization of SPION-decorated N-Ex

Considering that the retention of the administrated N-Ex in the liver and spleen may hinder their therapeutic efficacy, we then decorated N-Ex with SPIONs by transferrin (Tf)–transferrin receptor (TfR) interaction to improve their tumor-targeting capability (*21*, *22*). The magnetic behavior of Tf-SPION is shown in fig. S15A, confirming the successful immobilization of magnetic nanoparticles. Moreover, the homogeneously dispersed SPION adhered to the wall of vials quickly and resulted in the formation of a clear and transparent solution when an external magnetic field (MF) was applied (fig. S15B). The morphology of SPION represented a black dot structure as imaged by TEM (fig. S16A). The decoration of Tf to SPION was detected using an ultraviolet spectrophotometer (fig. S16B), and the particle size of Tf-SPION was measured by DLS (fig. S16, C and D). We then incubated Tf-SPION with the N-CM under an external MF to prepare for SPION-conjugated N-Ex (SPION-Ex; Fig. 3A and fig. S17). This procedure improved the separation efficiency of N-Ex and maintained a good dispersion of N-Ex in PBS and serum (fig. S18, A and B). The purified SPION-Ex was detected by TEM, and the TEM images showed that the spherical exosomes were surrounded by multiple superparamagnetic nanoparticles (Fig. 3B). The average size and zeta potential of SPION-Ex were 140 ± 11 nm and −34 ± 1 mV, respectively (Fig. 3, C and D). Furthermore, SPION-Ex displayed a good polydispersity, with a PDI lower than 0.3 (Fig. 3E). Western blot results confirmed the presence of exosomal markers, the enrichment of TfR, and the absence of calnexin in SPION-Ex (Fig. 3F). The purified SPION-Ex was labeled with DiR and incubated with HGC27 cells for 24 hours. Fluorescence confocal laser microscopy and imaging flow cytometry were used to visualize the intracellular localization of SPION-Ex. As shown in Fig. 3 (G and H), a stronger fluorescence signal (red) was observed in the cytoplasm of cells when incubated with DiR-labeled SPION-Ex under an external MF, indicating that SPION modification improved the uptake of N-Ex by the recipient cells. Overall, we have developed a SPION-based system for the rapid isolation and purification of N-Ex.

In vitro cytotoxicity of SPION-Ex

We then assessed the targeting ability of SPION-Ex in vitro. HGC27 cells were cultured with SPION-Ex (40 μg/ml) for 24 hours in the presence or absence of an external MF (fig. S19A). The responses of HGC27 cells to SPION-Ex treatment were monitored by CCK-8 assay. As shown in Fig. 4A, SPION-Ex/MF displayed a higher cytotoxicity toward HGC27 cells than the unmodified N-Ex and SPION-Ex without MF. Similarly, SPION-Ex/MF also exhibited a stronger inhibition of cell proliferation in other tumor cells (fig. S19B). Nevertheless, SPION-Ex/MF showed no toxicity to normal cells even when an external MF was applied (fig. S19C).

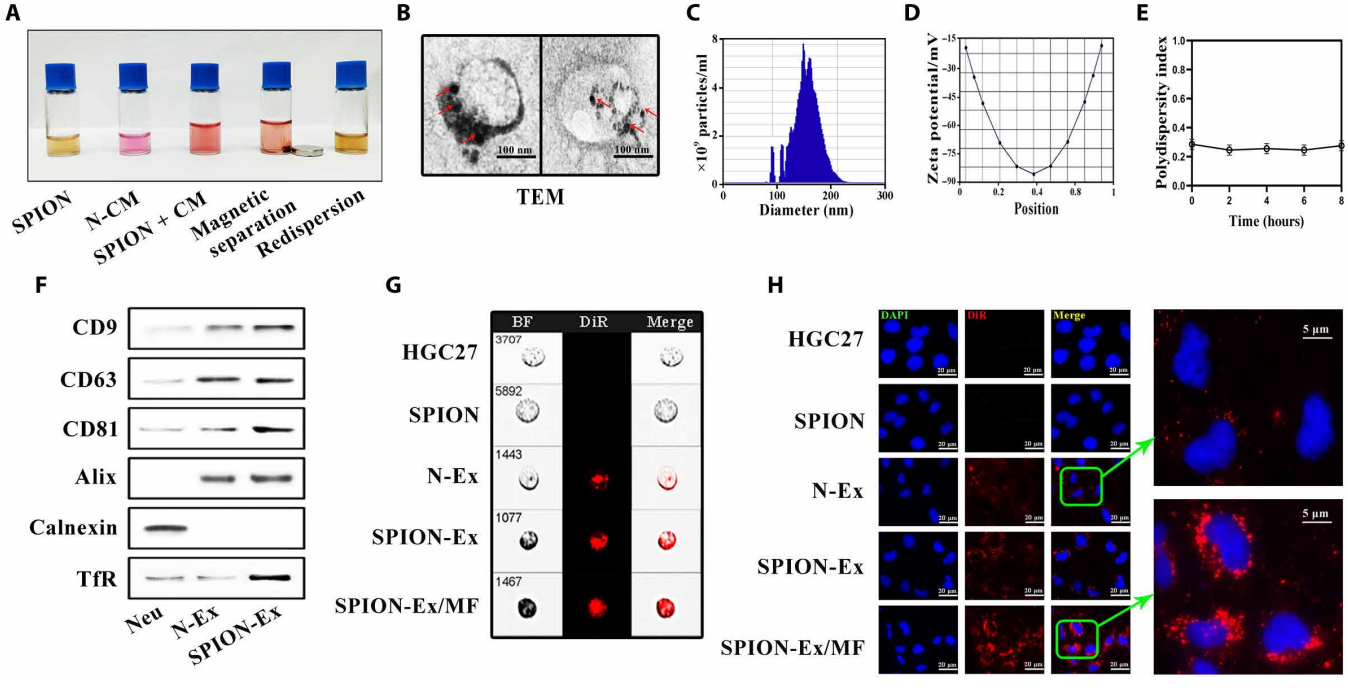

Fig. 3. Magnetic separation and characterization of SPION-Ex. (**A**) The procedure for magnetic separation of SPION-Ex. The CM of neutrophils was incubated with Tf-SPION solution (0.5 mg/ml; containing ~0.1 mg of SPION) for 4 hours at 4°C. (**B**) Representative TEM images of SPION-Ex. The red arrows indicate the SPION on the surface of exosomes. Scale bars, 100 nm. (**C** and **D**) The size distribution (C) and zeta potential (D) of SPION-Ex were measured by NTA. (**E**) The PDI of SPION-Ex was detected by DLS at the indicated times. (**F**) The expression of exosomal biomarkers (CD9, CD63, CD81, and Alix), ER marker (calnexin), and TfR in N-Ex was determined by Western blot. (**G** and **H**) The uptake of DiR-labeled SPION-Ex (red fluorescence) by HGC27 cells in the presence or absence of MF was examined by imaging flow cytometry (G) and fluorescence confocal laser microscopy (H). Scale bars, 20 μm.

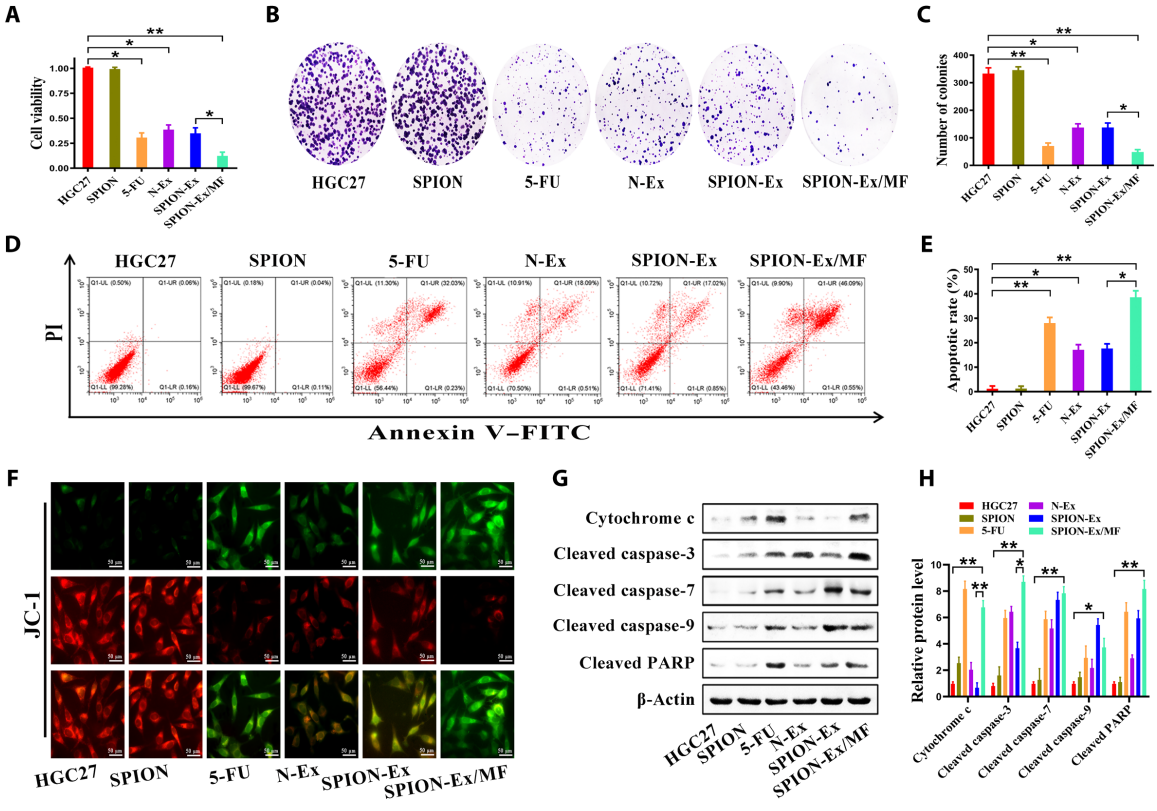

Fig. 4. Improved therapeutic effect of SPION-Ex in vitro. HGC27 cells were treated with PBS, SPION (100 μg/ml), 5-fluorouracil (5-FU) (30 μg/ml), N-Ex (40 μg/ml), and SPION-Ex (40 μg/ml) with or without MF for 24 hours. 5-FU was used as a positive control. (**A**) Cell viability of HGC27 cells was determined by CCK-8 assay. (**B** and **C**) Cell colony formation assays for HGC27 cells. (**D** and **E**) Cell apoptosis for HGC27 cells was determined by flow cytometry with annexin V/PI double staining. (**F**) JC-1 staining was used to detect the mitochondrial membrane potential of HGC27 cells. Scale bars, 50 μm. (**G** and **H**) Western blot assays for the expression of proteins in apoptosis signaling pathway in HGC27 cells. One-way ANOVA for multiple groups were applied for statistical analysis. *$P < 0.05$ and **$P < 0.01$.

The results of cell colony formation assay showed that tumor cells treated with SPION-Ex/MF (40 μg/ml) formed obviously smaller and fewer colonies than control cells, and this effect was more significant than that of 5-fluorouracil (5-FU) (30 μg/ml; Fig. 4, B and C). Flow cytometry results showed that SPION-Ex/MF (40 μg/ml) induced an increased percentage of apoptotic cells than 5-FU (30 μg/ml), N-Ex (40 μg/ml), and SPION-Ex (40 μg/ml) without MF (Fig. 4, D and E). JC-1 staining results also confirmed that SPION-Ex/MF most notably reduced the mitochondrial membrane potential of tumor cells as compared to 5-FU, N-Ex, and SPION-Ex without MF (Fig. 4F). The increased expression of cytochrome c and cleaved caspase-3 was also observed in the SPION-Ex/MF group, indicating that SPION-Ex more efficiently promoted cell apoptosis when an external MF was applied (Fig. 4, G and H). Overall, these data suggest that SPION-Ex/MF exerts an improved antitumor effect in vitro.

In vivo tumor-targeting and therapeutic effect of SPION-Ex

We next used a subcutaneous xenograft tumor model established by HGC27 cells in BALB/c nude mice to investigate the tumor-targeting ability and therapeutic response of SPION-Ex. When the tumor size reached ~50 mm^3, the mice were divided into three groups (PBS, SPION-Ex without MF, and SPION-Ex/MF; $n = 4$ per group). DiR-labeled SPION-Ex was intravenously injected into the mice (5 mg/kg of body weight; 100 μl), and the biodistribution of SPION-Ex under an external MF was visualized at different times after injection (12, 24, 48, and 72 hours) by an in vivo imaging system (IVIS). As depicted in Fig. 5A, the stronger fluorescence signals of DiR-labeled SPION-Ex were measured in tumors under MF, and the fluorescence signals mainly localized at the tumor site at 72 hours after injection. After in vivo imaging, the major organs and tumor tissues were excised for ex vivo imaging. Consistent with the in vivo imaging results, DiR-SPION-Ex was predominantly accumulated in the tumors (with MF), and the accumulation was time dependent (Fig. 5B and fig. S20), which demonstrated that SPION-Ex/MF had a remarkable tumor-targeting ability.

We further examined the antitumor efficacy of SPION-Ex/MF in another set of tumor-bearing mice ($n = 5$ per group). The mice were divided into six groups and received different treatments (PBS; SPION, 2 mg/kg of body weight; 5-FU, 5 mg/kg of body weight; N-Ex, SPION-Ex, and SPION-Ex/MF, 5 mg/kg of body weight; 100 μl) at 12, 16, 20, 24, 28, 32, and 36 days after tumor inoculation. The tumor size results showed that treatment with SPION-Ex under an external MF efficiently suppressed tumor growth in vivo (Fig. 5, C to E). Compared with the SPION-Ex without MF group, the treatment with SPION-Ex/MF showed an increased therapeutic effect. The survival rates of mice in different groups are shown in Fig. 5F. The average survival times of mice in the PBS, SPION, 5-FU, N-Ex, and SPION-Ex without MF groups were 45, 47, 67, 61, and 59 days, respectively. The mice treated with SPION-Ex/MF survived 86 days, and 40% of mice survived to the end of the study. The body weights of mice in

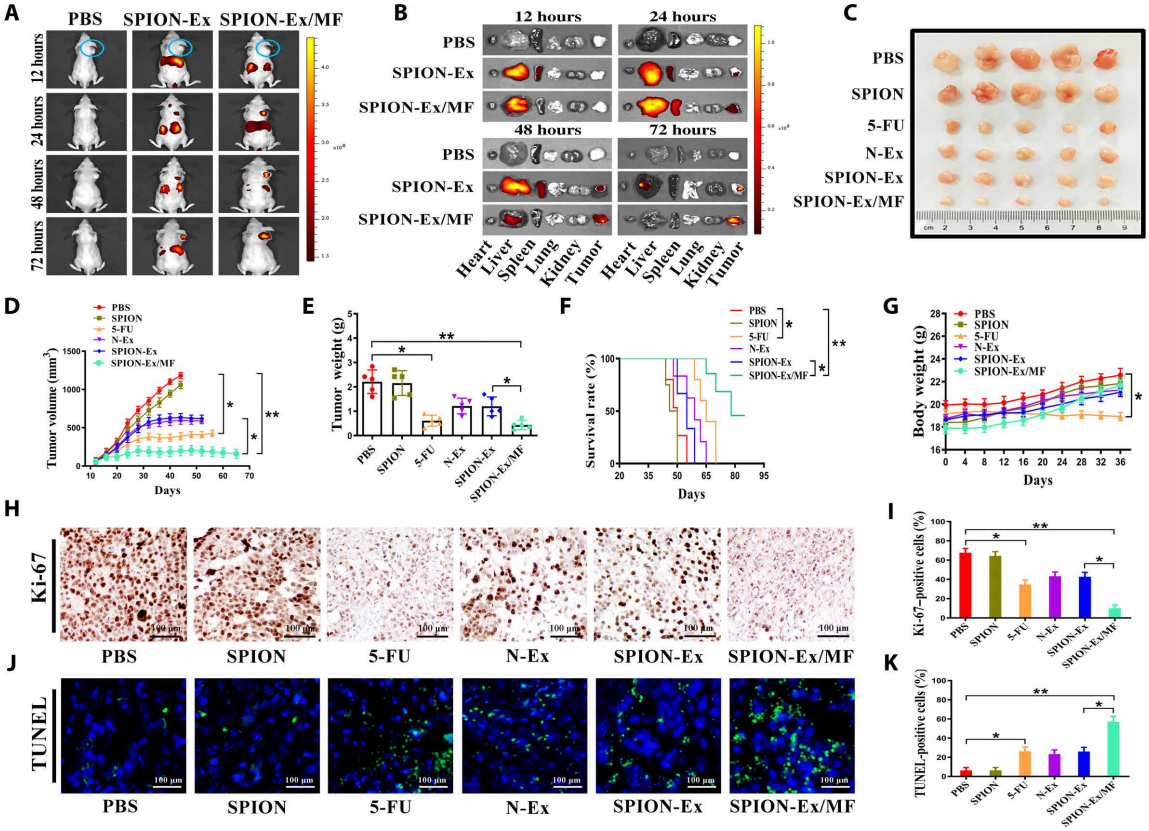

Fig. 5. Tumor-targeting ability and the therapeutic effect of SPION-Ex in vivo. (**A**) Representative images of the distribution of DiR-labeled SPION-Ex (5 mg/kg of body weight) in BALB/c nude mice under an external MF at 12, 24, 48, and 72 hours after intravenous injection ($n = 4$ per group). The circles indicate the tumor sites. (**B**) Representative images of the ex vivo fluorescence signals of DiR-labeled SPION-Ex (5 mg/kg of body weight) in major organs (liver, spleen, lung, heart, and kidney) and tumors at 12, 24, 48, and 72 hours after intravenous injection. (**C**) Representative images of subcutaneous xenograft tumors established by HGC27 cells in BALB/c nude mice ($n = 5$ per group) that received different treatments including PBS, SPION (2 mg/kg of body weight), 5-FU (5 mg/kg of body weight), N-Ex (5 mg/kg of body weight), and SPION-Ex (5 mg/kg of body weight) with or without MF. (**D**) Tumor growth was routinely examined, and the tumor growth curves in each group were shown. (**E**) The weights of the harvested xenograft tumors. (**F**) Survival rates of mice that received different treatments as indicated. (**G**) The body weights of mice at the end of study were shown. (**H** and **I**) Ki-67 staining of tumors from mice that received different treatments including PBS, SPION (2 mg/kg of body weight), 5-FU (5 mg/kg of body weight), N-Ex (5 mg/kg of body weight), and SPION-Ex (5 mg/kg of body weight) with or without MF. Scale bars, 100 μm. (**J** and **K**) TUNEL staining of tumors from mice that received different treatments including PBS, SPION (2 mg/kg of body weight), 5-FU (5 mg/kg of body weight), N-Ex (5 mg/kg of body weight), and SPION-Ex (5 mg/kg of body weight) with or without MF. Scale bars, 100 μm. One-way ANOVA for multiple groups were applied for statistical analysis. *$P < 0.05$ and **$P < 0.01$.

the SPION-Ex/MF group were comparable to that of the PBS group, while mice in the 5-FU group exhibited a notable decrease in body weight after treatment (Fig. 5G).

We further evaluated the safety of SPION-Ex/MF by collecting major organs from mice at 3 days after the last injection. The results of H&E staining revealed that there were congestion and irregular thickening of myocardial fibers and pulmonary capillaries in the 5-FU group, while no notable lesions were observed in the SPION-Ex/MF group (fig. S21). The results of blood biochemical tests showed that the serum levels of indicators for heart (CK, CK-MB, LDH, and α-HBDH), liver (ALT and AST), and kidney (BUN and CREA) functions increased in the 5-FU group but not in the SPION-Ex/MF group, suggesting that treatment with SPION-Ex/MF did not result in toxicity to major organs (fig. S22). The results of Ki-67 and TUNEL staining showed that there were less Ki-67–positive cells (Fig. 5, H and I) but more TUNEL-positive apoptotic cells (Fig. 5, J and K) in the SPION-Ex/MF group than the SPION-Ex without MF group. Moreover, the fluorescence signals in the cryosections of liver in the SPION-Ex/MF group were lower than that in the N-Ex and SPION-Ex without MF groups (fig. S23). These findings indicate that SPION-Ex/MF has a stronger targeted therapy effect than unmodified N-Ex and better safety than 5-FU in vivo.

Antitumor effect of SPION-NNV-DOX

Exosome-mimetic NVs have been reported as convenient and reliable drug nanocarriers. We then tested the possibility of NNV to be used as a drug delivery vehicle. To this end, we produced DOX-loaded cationic liposomes (DOX-CL) with a mass ratio of 3.9% (3.9 mg of drugs in 100 mg of liposomes) (fig. S24, A and B). We then incubated DOX-CL with neutrophils to generate DOX-carrying neutrophils and produced NNV-DOX by a serial extrusion method. The effects of NNV on the proliferation of tumor cells and normal cells were detected by CCK-8 assay (fig. S25, A and B). In similar to N-Ex, NNV also inhibited the proliferation of HGC27 cells in a dose-dependent manner but did not affect the viability of HUVECs. Western blot results showed that several representative proteins [CXCR4, intercellular adhesion molecule–1 (ICAM-1), L-selectin, and β1 integrin] in neutrophils were also preserved on NNV

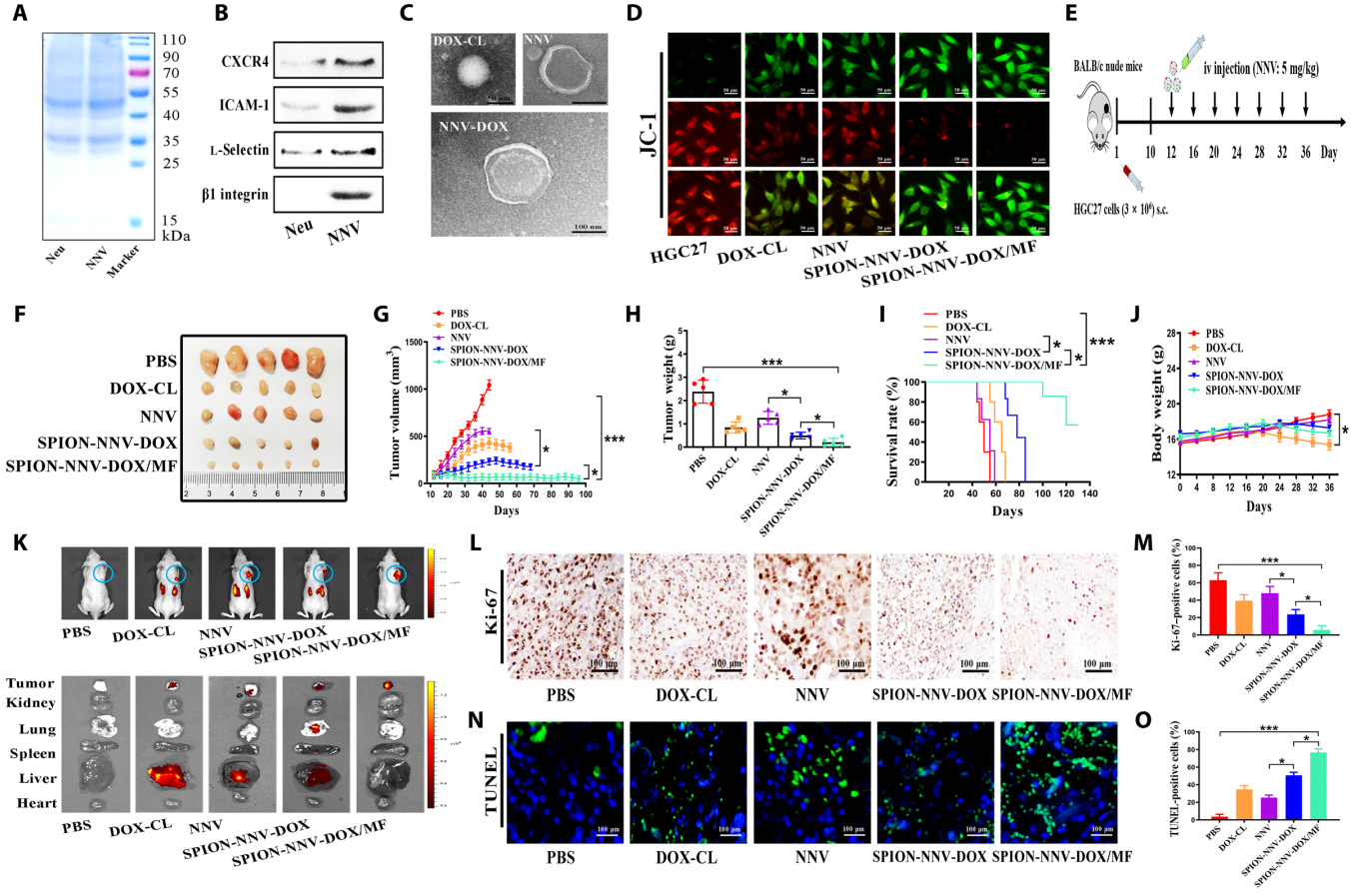

Fig. 6. SPION-modified, N-Ex–like NVs deliver DOX to inhibit tumor growth. (**A**) Protein profiles of neutrophils and its derived NNV were determined by SDS–polyacrylamide gel electrophoresis. (**B**) Western blot analyses of neutrophil membrane–specific proteins including CXCR4, ICAM-1, L-selectin, and β1 integrin in the NNV. (**C**) Neutrophils incubated with DOX-CL (50 μg/ml) were collected to prepare for NVs that encapsulated DOX (NNV-DOX). The morphology of DOX-CL, NNV, and NNV-DOX were examined by TEM. Scale bar, 100 nm. (**D**) The effects of DOX-CL (50 μg/ml), NNV (40 μg/ml), and SPION-NNV-DOX (40 μg/ml) with or without MF on the mitochondrial membrane potential of HGC27 cells at 24 hours after the treatment were detected by JC-1 staining. (**E**) Schematic design for SPION-NNV-DOX treatment in subcutaneous HGC27 xenograft tumor model in BALB/c nude mice. iv, intravenous; sc, subcutaneous. (**F** and **G**) Images and sizes of subcutaneous xenograft tumors in mice treated with PBS, DOX-CL (5 mg/kg of body weight), NNV (5 mg/kg of body weight), and SPION-NNV-DOX (5 mg/kg of body weight, DOX) with or without MF under a 24-day treatment regimen ($n = 5$ per group). (**H**) Tumor weights of mice that received different treatments as indicated. (**I**) Survival rates of mice that received different treatments as indicated. (**J**) Body weights of mice in each group at the end of the experiment. (**K**) Represent images of ex vivo distribution of DiR-labeled SPION-NNV-DOX/MF (5 mg/kg of body weight) in major organs and tumors of mice at 3 days after the last injection. (**L** and **M**) Ki-67 staining of tumors from mice that received different treatments. Scale bars, 100 μm. (**N** and **O**) TUNEL staining for tumors from mice in different groups. Scale bars, 100 μm. One-way ANOVA for multiple groups were applied for statistical analysis. *$P < 0.05$ and ***$P < 0.001$.

(Fig. 6, A and B). Neutrophils were incubated with DOX-CL (50 μg/ml), and the uptake of DOX-CL by neutrophils was detected via multidimensional imaging flow cytometry (fig. S26, A and B). The DOX-CL/neutrophil suspension was physically extruded 11 times by using a mini extruder to generate a large scale of NNV-DOX. The loading efficiency of DOX-CL into NNV after serial extrusion of neutrophils was 8.5%. TEM analysis showed that NNV-DOX displayed a typical core-shell structure with a single dimmer neutrophil membrane layer (Fig. 6C). The average size and zeta potential of NNV was 181 ± 9 nm and −16 ± 3 mV, and that of NNV-DOX was 230 ± 10 nm and −19 ± 1 mV, as detected by DLS (fig. S27, A to C). In addition, NNV expressed exosomal markers but not the ER marker (fig. S27D), indicating that NNV maintained the characteristics of N-Ex (*23*, *24*). Furthermore, Western blot results showed that FasL, granzyme A, granzyme B, and perforin were expressed in NNV as well (fig. S27E). A PDI of less than 0.3 was also observed in NNV and NNV-DOX (fig. S27F). The amounts of DOX released from NNV-DOX at different solutions were tested by high-performance liquid chromatography (HPLC). Compared with neutral environment (pH 7.4), the acidic environment (pH 5.5) accelerated the release of DOX, showing about 45% (pH 7.4) and 74% (pH 5.5) accumulative release at 72 hours after incubation, respectively (fig. S28, A and B).

We further modified NNV-DOX with Tf-SPION (SPION-NNV-DOX) to improve their tumor-targeting ability. As shown in fig. S29A, SPION-NNV-DOX/MF displayed a higher cytotoxicity toward HGC27 cells than SPION-NNV-DOX without MF. Moreover, the antitumor activities of N-Ex, SPION-Ex, NNV, NNV-DOX, and SPION-NNV-DOX (with or without MF) were compared, and the results showed that NNV had a similar effect to N-Ex and DOX

loading improved its cytotoxicity (fig. S29B). The mitochondrial membrane potential of HGC27 cells in the SPION-NNV-DOX/MF group was significantly decreased compared to DOX and NNV alone groups (Fig. 6D).

We then evaluated the antitumor effect of SPION-NNV-DOX/MF on a mouse xenograft tumor model established by HGC27 cells in BALB/c nude mice (Fig. 6E). Once the tumor grew to about 50 mm^3, the mice were intravenously injected with PBS, DOX-CL (5 mg/kg of body weight), NNV (5 mg/kg of body weight), and SPION-NNV-DOX (5 mg/kg of body weight, DOX; with or without MF) for 7 cycles (4 days/cycle). Compared with DOX, NNV, and SPION-NNV-DOX without MF, SPION-NNV-DOX/MF exhibited the strongest tumor growth inhibition effect (Fig. 6, F to H). SPION-NNV-DOX/MF significantly prolonged the median survival time of mice from 65 (DOX-CL), 58 (NNV), and 82 (SPION-NNV-DOX) to 140 days (SPION-NNV-DOX/MF) (Fig. 6I). Moreover, the body weights of mice in the SPION-NNV-DOX/MF group were not significantly changed, indicating the safety of this treatment (Fig. 6J). In addition, the fluorescence signals of the SPION-NNV-DOX/MF (DiR-labeled NNV; red fluorescence) group mainly accumulated at the tumor site, and the marginal fluorescent signal was observed in the liver at 3 days after the last injection (Fig. 6K and fig. S30). Ki-67 and TUNEL staining results showed that SPION-NNV-DOX/MF inhibited tumor cell proliferation and induced cell apoptosis in tumor tissues to the greatest extent compared to other groups (Fig. 6, L to O). The results of H&E staining and blood biochemical tests indicated that SPION-NNV-DOX/MF had few toxic and side effects, while DOX-CL showed remarkable alterations to the histology of major organs and expression levels of indicators for liver, kidney, and heart functions (figs. S31 and S32).

To further prove that SPION-NNV is a promising platform for the delivery of DOX and treatment of cancer, we constructed another subcutaneous xenograft tumor model in severely immunodeficient NCG mice. SW480 cells (4×10^6 cells per mouse) were subcutaneously implanted into NCG mice ($n = 7$ per group) and treated as described above (Fig. 7A). We confirmed that the effects of SPION-NNV-DOX/MF on SW480 cell proliferation and apoptosis in vitro were superior to that of free DOX, SPION-Ex, SPION-Ex/MF, SPION-NNV, SPION-NNV/MF, and SPION-NNV-DOX without MF (figs. S33 and S34). In vivo biodistribution data showed that the fluorescence signals of SPION-NNV-DOX/MF mostly accumulated in the tumor (Fig. 7B and fig. S35). Tumor volume and tumor

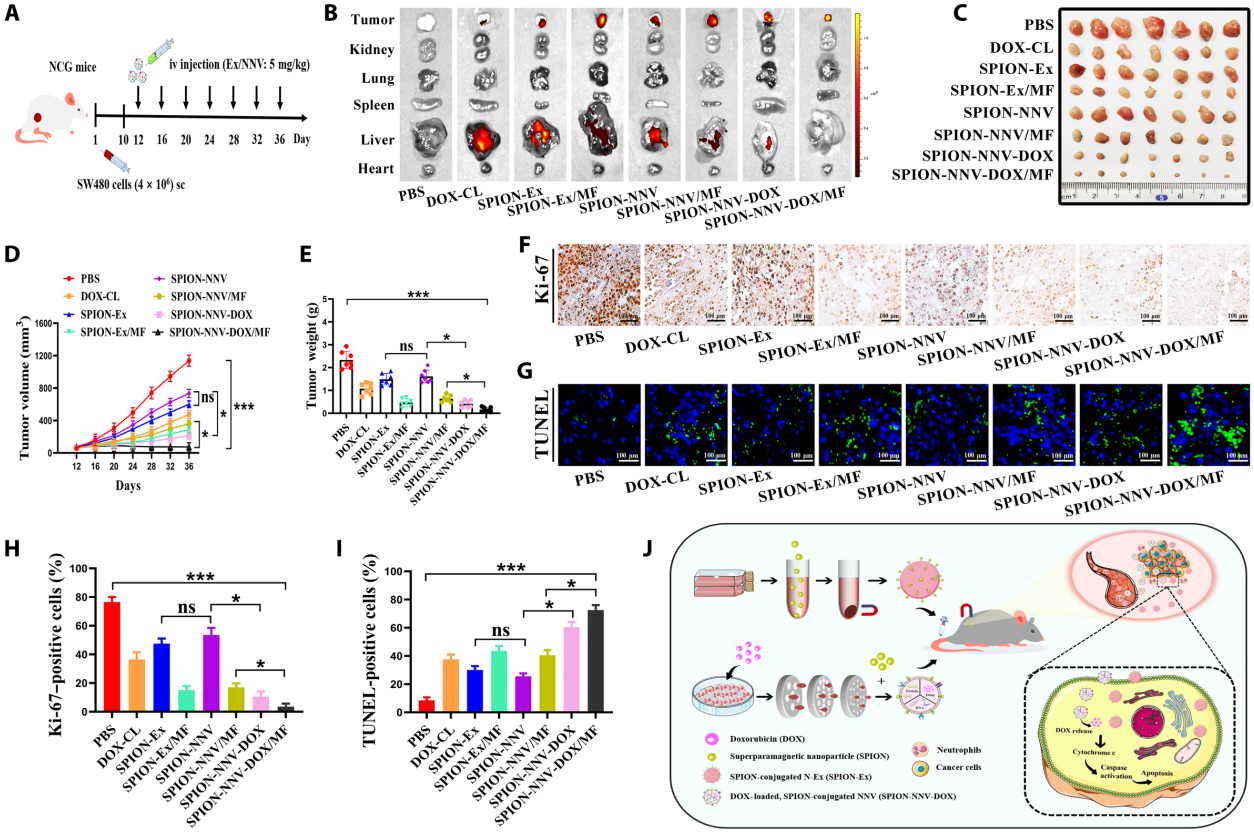

Fig. 7. Therapeutic effect of SPION-NNV-DOX on tumor-bearing NCG mouse. (**A**) Schematic design for SPION-NNV-DOX treatment in subcutaneous xenograft tumor model established by SW480 cells in NCG mice. (**B**) Representative images of ex vivo fluorescent signals in the major organs (heart, liver, spleen, lung, and kidney) and tumors of mice at 3 days after the last injection. (**C**) Images of SW480 xenograft tumors in NCG mice treated with PBS, DOX-CL (5 mg/kg of body weight), SPION-Ex (5 mg/kg of body weight) with or without MF, SPION-NNV (5 mg/kg of body weight) with or without MF, and SPION-NNV-DOX (5 mg/kg of body weight, DOX) with or without MF under 7 cycles of treatment regimen ($n = 7$ per group; 4 days/cycle). (**D**) Tumor volume was closely monitored and tumor growth curves were recorded. (**E**) Tumor weights of mice in each group at the end of study (day 39). (**F** and **G**) Representative images of Ki-67 (F) and TUNEL (G) staining of tumors in each group. (**H** and **I**) Statistical analyses of immunohistochemical staining results. (**J**) Schematic illustration of SPION-Ex and exosome-like NVs as a novel cancer therapeutic agent and drug delivery nanoplatform. Scale bars, 100 μm. One-way ANOVA for multiple groups were applied for statistical analysis. *$P < 0.05$ and ***$P < 0.001$.

weight results showed that SPION-NNV-DOX/MF suppressed tumor growth more efficiently than DOX-CL, SPION-Ex, SPION-Ex/MF, SPION-NNV, SPION-NNV/MF, and SPION-NNV-DOX without MF (Fig. 7, C to E). Furthermore, the number of Ki-67–positive cells was significantly decreased and the number of TUNEL-positive cells was notably increased after treatment with SPION-NNV-DOX/MF compared with other groups (Fig. 7, F to I). DOX-CL treatment resulted in a decrease in mouse body weight and led to toxicity in major organs, while SPION-NNV-DOX/MF treatment had minimal side effect (figs. S36 and S37). In summary, NNV was used as a novel nanoparticle platform to deliver DOX for higher tumor-targeting and improved therapeutic response.

DISCUSSION

In this study, we isolated exosomes from the peripheral blood neutrophils of healthy donors and showed that N-Ex exerted cytotoxicity against tumor cells by activating apoptosis signaling pathway. We also developed a quick magnetic separation method to isolate exosomes from neutrophils and endowed N-Ex with dual tumor-targeting abilities (biological targeting and magnetic targeting), which greatly improved their therapeutic efficacy. Moreover, we fabricated NNVs at high yield, as a new delivery tool for chemotherapeutic drugs. We showed that, through this strategy, SPION-decorated, DOX-loaded NNV achieved dual therapeutic effects (both drug and NNV), which almost completely eliminated tumor growth in mice. These findings not only demonstrate the role of exosomes in the antitumor activity of neutrophils but also provide natural and biomimetic N-Ex as a new cancer therapeutic agent and drug delivery nanoplatform.

Previous studies demonstrate that immune cell–derived exosomes have a potent role in cancer therapy (*25*). In line with these studies, we found that exosomes from neutrophils also showed high cytotoxicity to tumor cells but not normal cells and significantly restricted tumor growth in BALB/c nude mice. Recently, Wang *et al.* (*26*) reported that neutrophil-exosomes carrying the drug could rapidly penetrate the blood-brain barrier and migrate into the brain (*26*). Intravenous injection of DOX loaded neutrophil-exosomes efficiently suppressed tumor growth and prolonged survival time in a glioma mouse model. We found that most N-Ex localized in the liver and few N-Ex accumulated at the tumor site after intravenous injection. Therefore, we improved the targeting ability of N-Ex to increase their use for cancer therapy. SPIONs have been widely used in cancer therapy for their excellent superparamagnetism property (*27*, *28*). The conjugation of SPIONs with exosomes has many advantages, including magnetic targeted functionalization, magnetic thermotherapy, and delivery of anticancer agents. Zhuang *et al.* (*29*) showed that SPION-loaded exosomes enhanced cancer targeting and significantly suppressed tumor growth when an external MF was applied. Previous studies demonstrate that iron oxide nanoparticle–modified EVs can be rapidly separated from the cell culture medium and blood, which significantly enhances the antitumor efficacy of the loaded drug in mouse tumor models (*30*, *31*). We anchored the carboxylated modified SPIONs onto N-Ex via Tf-TfR interaction, as described previously (*31*, *32*). The isolation of SPION-Ex from neutrophil supernatant under an external MF (1 T) was faster than the ultracentrifugation method. The purified SPION-Ex was immediately redispersed in PBS and showed an excellent stability for 7 days. Moreover, SPION-Ex under the external MF (SPION-Ex/MF) displayed a higher accumulation at the tumor site after intravenous injection and exerted a stronger targeted therapy effect than the unmodified ones. In addition, SPION-Ex/MF exerted a comparable antitumor activity to the commonly used chemotherapeutic drug 5-FU but showed no toxic effect to normal organs such as loss of body weight and impaired liver, kidney, and heart functions, suggesting that we have developed a dual-functional exosome-based SPION cluster as a targeted and safe agent for cancer therapy (*33*, *34*).

Bioinspired exosome-mimetic NVs have been developed to deliver chemotherapeutic drugs for cancer therapy (*35*). For instance, Jang *et al.* (*17*) have generated high quantities of exosome-mimetic NV from monocytes/macrophages that have similar characteristics with exosomes but have 100-fold higher production yield. Chemotherapeutic drug–loaded NV traffics to tumor site and reduces tumor growth more efficiently than free drug and liposome formulation, while showing low adverse effects, suggesting that the bioengineered NV can serve as a novel exosome mimetic for anticancer drug delivery (*36*, *37*). Similarly, Yong *et al.* (*38*) have developed tumor cell–derived EV-mimetic porous silicon nanoparticles (PSiNPs) for targeted cancer therapy. These EV-based DOX-loaded PSiNPs mainly accumulated in the tumor site and exhibited enhanced antitumor activities in multiple cancer models. The use of neutrophils as a living cell drug delivery system and neutrophil cell membrane–coated nanoparticles as a biomimetic drug delivery system have been tested as new strategies for many diseases, including cancer (*39*–*41*). Xue *et al.* (*42*) demonstrated that neutrophils carrying paclitaxel could overcome the blood-brain barrier and inhibited the recurrence of glioma after surgical tumor resection. Here, we produced N-Ex–like NVs and used them as nanocarriers for chemotherapeutic drugs. Zhang *et al.* (*30*) have developed magnetic and folate-modified microvesicles (FA/IONP-MVs) and loaded them with DOX to generate the FA/IONP-MVs-DOX delivery platform, which was rapidly isolated from the supernatant and exhibited significantly enhanced antitumor efficacy both in vitro and in vivo. Inspired by this strategy, we engineered NNV-DOX with SPION to form a magnetic drug delivery system. Our results showed that SPION-NNV-DOX under an external MF has enhanced targeting ability to tumor site after systemic administration. The SPION-NNV-DOX/MF greatly suppressed tumor growth and significantly prolonged the survival of BALB/c nude mice and NCG mice, suggesting that magnetism-modified NNV provides efficient drug delivery and dual tumor-targeting response.

In conclusion, we reported here that neutrophils exerted an antitumor effect via exosomes. N-Ex promoted tumor cell death by activating the apoptosis signaling pathway. Taking advantage of the superparamagnetic nanoparticles, we isolated exosomes from the neutrophil supernatant rapidly and endowed them with high tumor-targeting capability, which significantly enhanced their antitumor activity. We also developed a DOX-loaded, SPION-modified, N-Ex–like NV system that specifically targeted the tumor site and exerted dual antitumor effects (Fig. 7J). Together, the engineered N-Ex and exosome-like NVs provide a powerful cancer therapeutic agent and an efficient and safe drug delivery nanoplatform for cancer therapy.

MATERIALS AND METHODS

Experimental reagents

Carboxyl group–functionalized SPION and DOX-CL were purchased from Xi'an Ruixi Biological Technology (China). A mini

extruder and polycarbonate membrane filters with different pore sizes were also bought from Xi'an Ruixi Biological Technology. 5-FU was obtained from Sigma-Aldrich (USA). CCK-8, DiR, 4′,6-diamidino-2-phenylindole (DAPI), and annexin V–fluorescein isothiocyanate (FITC)/propidium iodide (PI) cell apoptosis kit were purchased from Vazyme (China). BCA protein assay kit and mitochondrial membrane potential kit (JC-1) were obtained from Thermo Fisher Scientific (USA). Cell culture media, fetal bovine serum (FBS), and 1% penicillin/streptomycin were purchased from HyClone (USA). TUNEL staining kit was obtained from Roche (Germany).

Cell culture

Cells were cultured in Dulbecco's modified Eagle's medium and RPMI 1640 supplemented with 10% of FBS at 37°C in a humidified atmosphere containing 5% CO_2. Human gastric mucosal cells (GES-1), HUVEC, HFL, human gastric cancer cells (HGC27), human hepatoma cells (HepG2) and human colon cancer cells (SW480) were purchased from the Institute of Biochemistry and Cell Biology at the Chinese Academy of Sciences (China).

Isolation and characterization of exosomes

Neutrophils were isolated from the peripheral blood by using polymorphprep. The cells were cultured in RPMI 1640 supplemented with 10% of FBS (exosome-depleted) at 37°C, and the CM was collected for 24 hours. Then, the CM was centrifuged at 500*g* for 10 min, 2000*g* for 10 min, and 12,000*g* for 30 min to remove cells and cell debris. The supernatants were pelleted by ultracentrifugation at 100,000*g* for 80 min. N-Ex were dissolved with PBS and stored at −80°C until use. Protein concentration was determined by the BCA protein assay kit.

The morphology of N-Ex was identified by TEM (Philips, Netherlands) and AFM (Veeco DM3100, USA). Exosomal markers CD9, CD63, CD81 [1:1000; Cell Signaling Technology (CST), USA], and Alix (1:1000; Abcam, UK) and the ER marker calnexin (1:1000; Abcam, UK) were detected by Western blot. The size distribution and zeta potential of N-Ex were measured by the NanoSight LM10 system (NTA, UK). The PDI of N-Ex was tested by DLS (Malvern Instruments, UK).

Cellular uptake assay

Cells were seeded in 12-well plates (2×10^5 cells per well) and incubated for 12 hours. The membrane fluorescent dye DiR (5 μM) was cocultured with N-Ex or SPION-Ex for 30 min at 37°C, and the mixed samples were washed twice with PBS and centrifuged at 100,000*g* for 80 min. DiR-labeled N-Ex (40 μg/ml) or SPION-Ex (40 μg/ml) was added into the culture medium of tumor cells. Then, cells were fixed with 4% of paraformaldehyde for 30 min and permeabilized in 0.2% of Triton X-100 for 5 min. The cell nuclei were stained by DAPI for 10 min. Cellular uptake of N-Ex or SPION-Ex was examined with multidimensional panoramic flow cytometry (Flow Sight, USA) and fluorescence confocal laser microscopy (GE, USA).

Cell viability assay

The cytotoxicity of N-Ex against tumor cells (HGC27, SW480, and HepG2) and normal cells (GES-1, HUVEC, and HFL) was evaluated by CCK-8 assay. Cells were seeded in 96-well plates (3×10^3 cells per well) and allowed to attach overnight at 37°C. Various concentrations of N-Ex (20, 40, and 80 μg/ml) were added into the culture plates for 12, 24, 36, and 48 hours. The culture media of different groups were discarded, and CCK-8 solution was added into 96-well plates for 4 hours. Absorbance of each well was measured at 450 nm by using an enzyme-linked immunosorbent plate assay reader (FLX800, USA). For comparative study, the cell viability of tumor cells was evaluated by CCK-8 assay after different treatments, including N-Ex (40 μg/ml), PBMCs-Ex (40 μg/ml), SPION (100 μg/ml), 5-FU (30 μg/ml), SPION-Ex (40 μg/ml) with or without MF, DOX-CL (45 μg/ml), NNV (40 μg/ml), SPION-NNV (40 μg/ml) with or without MF, and SPION-NNV-DOX (40 μg/ml) with or without MF.

Cell apoptosis assay

The effects of N-Ex on cell apoptosis were assessed by using the annexin V–FITC/PI cell apoptosis kit. Tumor cells and normal cells (2×10^5 cells per well) were seeded in six-well plates and treated with N-CM, N-Ex (40 μg/ml), SPION (100 μg/ml), 5-FU (30 μg/ml), and SPION-Ex (40 μg/ml) with or without MF for 24 hours. After treatment, the cells were washed twice with cold PBS, centrifuged at 800 rpm for 5 min, and resuspended in 1× binding buffer. Cells were stained with 5 μl of annexin V–FITC and 5 μl of PI at room temperature. The stained cells were then analyzed by flow cytometry (FACSCalibur, BD).

Colony formation assay

Tumor cells and normal cells (800 cells per well) were seeded in six-well plates and allowed to attach overnight. Subsequently, the cells were treated with N-CM, N-Ex (40 μg/ml), SPION (100 μg/ml), 5-FU (30 μg/ml), N-Ex (40 μg/ml), and SPION-Ex (40 μg/ml) with or without MF for 24 hours and replaced with a new culture medium every 3 days. Last, the cells were fixed in 4% of paraformaldehyde and stained with 0.5% of crystal violet. The number of cell colony was calculated under a microscope (TE300, Japan).

Western blot

Total protein from cells and tumor tissues was obtained by using radioimmunoprecipitation assay lysis buffer containing protease inhibitor cocktail. Equal amounts of proteins from each group were separated by SDS–polyacrylamide gel electrophoresis and then transferred onto polyvinylidene difluoride membranes. After blocking with 5% of nonfat milk for 1 hour, the membranes were incubated with primary antibodies at 4°C overnight. The used antibodies included CD9, CD63, CD81, Alix, calnexin, FasL, granzyme A, granzyme B, perforin (1:500; CST, USA), cleaved caspase-3, cleaved caspase-7, cleaved caspase-9, cleaved PARP (1:1000; SAB, USA), cytochrome c (1:1000; Bioworld, USA), TfR (1:1000; CST, USA), CXCR4, ICAM-1, β1 integrin (1:1000; Abcam), L-selection (1:500; R&D Systems), and β-actin (1:2000; Abcam, USA). Horseradish peroxidase–conjugated goat anti-rabbit and goat anti-mouse antibodies (SAB, USA) were used to detect the bound primary antibodies. The signals were detected by the enhanced chemiluminescence reagent and analyzed by ImageJ software.

Detection of mitochondrial membrane potential

The mitochondrial membrane potential of tumor cells (HGC27, SW480, and HepG2) was examined by JC-1 probe. Cells were seeded in six-well plates (1×10^5 cells per well) and incubated with N-Ex (40 μg/ml), SPION (100 μg/ml), 5-FU (30 μg/ml), SPION-Ex (40 μg/ml) with or without MF, DOX-CL (45 μg/ml), NNV (40 μg/ml), SPION-NNV (40 μg/ml) with or without MF, and SPION-NNV-DOX

(40 μg/ml) with or without MF for 24 hours. Then, cells were loaded with JC-1 (1 mg/liter) for 20 min at 37°C. After washing with cold PBS, the fluorescence intensity of each group was analyzed by fluorescence confocal laser microscopy (GE, USA).

Antitumor efficacy in xenograft tumor models

All animal studies were performed by using 4- to 6-week-old female BALB/c nude mice and NCG mice (Model Animal Center of Nanjing University, China). HGC27 cells (3×10^6 cells per mouse) were subcutaneously injected into the flanks of BALB/c nude mice ($n = 5$ per group). Tumor volume and weight were assessed every 4 days, and tumor volumes were calculated as $V = 0.5 \times a \times b^2$, where V represents the volume, a represents the longitudinal diameter, and b represents the latitudinal diameter. The mice were divided into different groups randomly when the tumor sizes reached ~50 mm^3. N-Ex was intravenously or intratumorally (5 mg/kg of body weight; 100 μl) injected into BALB/c nude mice. To evaluate the antitumor efficacy of SPION-Ex in vivo, the BALB/c nude mice were intravenously injected with PBS, SPION (2 mg/kg of body weight; 100 μl), 5-FU (5 mg/kg of body weight; 100 μl), N-Ex, SPION-Ex (5 mg/kg of body weight; 100 μl), and SPION-Ex/MF (5 mg/kg of body weight; 100 μl) under an external MF (MF = 1 T). For drug delivery study, PBS, DOX-CL (5 mg/kg of body weight; 100 μl), NNV (5 mg/kg of body weight; 100 μl), SPION-NNV-DOX (5 mg/kg of body weight; 100 μl), and SPION-NNV-DOX/MF (5 mg/kg of body weight; 100 μl) under an external MF were injected into BALB/c nude mice by tail vein and treated every 4 days. In another set of experiments, NCG mice ($n = 7$ per group) were subcutaneously transplanted with 4×10^6 SW480 cells per mouse. NCG mice were treated with intravenous injection of PBS, DOX-CL (5 mg/kg of body weight; 100 μl), SPION-Ex (5 mg/kg of body weight; 100 μl) with or without MF, SPION-NNV (5 mg/kg of body weight; 100 μl) with or without MF, and SPION-NNV-DOX (5 mg/kg of body weight; 100 μl) with or without MF. The body weights and survival periods of each group were monitored during treatment. Mouse tissue samples (heart, liver, spleen, lungs, kidneys, and tumor) were collected and cut into 8-μm histology slices using a cryostat, and each section was dyed with DAPI. The distribution of fluorescent signals of N-Ex, SPION-Ex, and SPION-NNV-DOX in the major organs and tumors were detected by confocal laser microscopy. The protocol was approved by the Animal Use and Care Committee of Jiangsu University (2014280).

In vivo biodistribution and magnetic targeting of SPION-Ex

SPION-modified exosomes were labeled with DiR in pH 7.4 buffer solution, according to the manufacturer's instructions. The DiR-labeled SPION-Ex was washed three times with cold PBS, separated magnetically from the culture supernatant, and redispersed into PBS. HGC27 cells (3×10^6 cells per mouse) were subcutaneously injected into the flanks of the BALB/c nude mice ($n = 4$ per group). When the tumor volume reached ~50 mm^3, the mice were injected with DiR-labeled SPION-Ex, and an external MF was placed over the surface of the tumor using Steri-Strip tape. The biodistribution of DiR-labeled SPION-Ex under the external MF in tumor was recorded by an IVIS imaging system (IVIS 100, USA) at 12, 24, 48, and 72 hours after injection. The fluorescence imaging results and average radio intensities were recorded. At the end of study, the tumors were collected and cut into 5-mm histology slices, dyed with DAPI, and visualized by fluorescence confocal laser microscopy.

Immunohistochemistry

All the mice were euthanized at 3 days after the last injection. For immunohistochemical analyses, all the tumor tissues were embedded in paraffin and dissected into 4-μm sections. To assess the proliferation of tumor cells, tissue sections were incubated with primary monoclonal antibody against Ki-67 (1:200; CST, USA) overnight after blocking with goat serum for 1 hour. Then, tissue sections were incubated with horseradish peroxidase–conjugated secondary antibodies using a diaminobenzidine substrate kit (Dako, Glostrup, Denmark). The histology of tumor tissues was examined under an optical microscope (DP73; Tokyo, Japan).

TUNEL staining

Tumor sections were fixed in 4% of paraformaldehyde for 20 min and washed with cold PBS for 30 min. Then, the tumor slices were stained with TUNEL reaction mixture (50 μl) for 60 min at 37°C after washing with PBS. Last, the cell nuclei were stained with DAPI and visualized by fluorescence confocal laser microscopy.

Safety evaluation

The major organs of BALB/c nude mice and NCG mice were collected at 3 days after the last injection. For histological studies, all the tissue sections of the heart, liver, spleen, lung, kidney, and tumor were fixed with 10% of neutral buffered formalin. Then, paraffin-embedded continuous sections (4 μm) were stained with H&E to examine the pathological changes. All the images of tissue sections were observed by an inverted fluorescence microscope (CX41, Olympus, Japan). In addition, the blood samples of BALB/c nude mice were collected after treatment with different formulations. The quantities of liver function indexes (ALT and AST), renal function index (BUN and CREA), and myocardial zymogram (CK, CK-MB, LDH, and α-HBDH) in serum were determined by using an automatic serum chemical analyzer (AU5800, Beckman).

Magnetic separation and redispersion of SPION-Ex

The N-CM was centrifuged and filtered through a 0.22-μm filter membrane to remove dead cells and cell debris. For magnetic separation, 2 ml of N-CM was mixed with 100 μl of Tf-SPION solution (0.5 mg/ml; containing ~0.1 mg of SPION) and incubated for 4 hours at 4°C to allow the SPION to anchor onto exosomes via Tf-TfR interaction. Then Tf-SPION–labeled exosomes were separated from N-CM by an external magnet. SPION-Ex was obtained after discarding the culture medium and washed three times with PBS. Last, Tf-SPION–labeled exosomes were resuspended in PBS and stored at 4°C before use. To assess the stability of SPION-Ex, SPION-Ex was redispersed in PBS buffer and serum for different times. The hydrodynamic diameters of SPION-Ex in PBS buffer and serum were evaluated by DLS (Malvern Instruments, UK). The measurements of the two groups were done in triplicate, and the results were averaged.

Characterization of SPION-Ex

SPION-Ex was redispersed in 200 μl of PBS for 10 min, and the concentration of SPION-Ex was examined by using a micro BCA protein assay kit. The morphology of SPION-Ex was imaged by TEM. The particle size and zeta potential of SPION-Ex were measured by NanoSight LM10 system. The PDI of SPION-Ex was detected by DLS (Malvern Instruments, UK). The exosomal markers CD9, CD63, CD81 (1:1000; CST, USA), and Alix (1:1000; Abcam, UK), the ER

marker calnexin (1:1000; Abcam, UK), and TfR (1:1000; CST, USA) of the magnetic separation mixture were assayed by Western blot. All samples were measured in triplicate.

In vitro uptake of DOX by neutrophils

Liposome-loaded DOX (DOX-CL) was purchased from Xi'an Ruixi Biological Technology. The entrapment efficiency of DOX-CL was 15%. The particle size and zeta potential of DOX-CL were measured by DLS (Malvern Instruments, UK). Neutrophils (1×10^6 cells/ml) isolated from human peripheral blood were incubated with DOX-CL at a DOX concentration of 50 μg/ml. The uptake of DOX-CL (red fluorescence) by neutrophils was examined by multidimensional panoramic flow cytometry (Flow Sight, USA).

Preparation and characterization of SPION-NNV-DOX

Neutrophils were resuspended in PBS at a concentration of 5×10^6 cells/ml. The cell suspension was sequentially extruded 11 times through 1-μm, 400-nm, and 200-nm polycarbonate membrane filters by using a mini extruder (Avanti Polar Lipids, USA). To enrich NNVs, the extruded samples were ultracentrifuged at 100,000*g* for 80 min at 4°C. Then, the purified NNVs were dissolved with PBS and stored at −80°C until use.

Neutrophils were incubated with DOX-CL, and the NNV-DOX was obtained as described above. The amount of DOX released from NNV-DOX was detected by HPLC. The SPION-modified NNV-DOX was prepared and separated from the mixture by magnetic separation and stored at 4°C for further experiments. The particle size, zeta potential, and PDI of NNV and NNV-DOX were tested by DLS (Malvern Instruments, UK). Exosomal biomarkers CD9, CD63, CD81 (1:1000; CST, USA), and Alix (1:1000; Abcam, UK), the ER marker calnexin (1:1000; Abcam, UK), and TfR (1:1000; CST, USA) were detected by Western blot. The morphologies of DOX-CL, NNV, and NNV-DOX were observed by TEM.

Statistical analysis

All experiments were performed at least in triplicate of each group, and the statistical analyses were carried out by GraphPad Prism Software (version 7). The results were presented as mean values ± SD. One-way analysis of variance (ANOVA) and two-way ANOVA for multiple groups as well as Student's *t* test for two groups were applied for statistical analysis. Survival time was analyzed by the Kaplan-Meier method and log-rank test. $P < 0.05$ was considered statistically significant.

SUPPLEMENTARY MATERIALS

Supplementary material for this article is available at https://science.org/doi/10.1126/sciadv.abj8207

View/request a protocol for this paper from *Bio-protocol*.

REFERENCES AND NOTES

1. M. E. Shaul, Z. G. Fridlender, Tumour-associated neutrophils in patients with cancer. *Nat. Rev. Clin. Oncol.* **16**, 601–620 (2019).
2. S. Jaillon, A. Ponzetta, D. Di Mitri, A. Santoni, R. Bonecchi, A. Mantovani, Neutrophil diversity and plasticity in tumour progression and therapy. *Nat. Rev. Cancer* **20**, 485–503 (2020).
3. R. Kalluri, V. S. LeBleu, The biology, function, and biomedical applications of exosomes. *Science* **367**, eaau6977 (2020).
4. S. Munich, A. Sobo-Vujanovic, W. J. Buchser, D. Beer-Stolz, N. L. Vujanovic, Dendritic cell exosomes directly kill tumor cells and activate natural killer cells via TNF superfamily ligands. *Onco. Targets. Ther.* **1**, 1074–1083 (2012).
5. L. Zhu, S. Kalimuthu, P. Gangadaran, J. M. Oh, H. W. Lee, S. H. Baek, S. Y. Jeong, S. W. Lee, J. Lee, B. C. Ahn, Exosomes derived from natural killer cells exert therapeutic effect in melanoma. *Theranostics* **7**, 2732–2745 (2017).
6. P. Wang, H. Wang, Q. Huang, C. Peng, L. Yao, H. Chen, Z. Qiu, Y. Wu, L. Wang, W. Chen, Exosomes from M1-polarized macrophages enhance paclitaxel antitumor activity by activating macrophages-mediated inflammation. *Theranostics* **9**, 1714–1727 (2019).
7. L. Lugini, S. Cecchetti, V. Huber, F. Luciani, G. Macchia, F. Spadaro, L. Paris, L. Abalsamo, M. Colone, A. Molinari, F. Podo, L. Rivoltini, C. Ramoni, S. Fais, Immune surveillance properties of human NK cell-derived exosomes. *J. Immunol.* **189**, 2833–2842 (2012).
8. P. Neviani, P. M. Wise, M. Murtadha, C. W. Liu, C. H. Wu, A. Y. Jong, R. C. Seeger, M. Fabbri, Natural killer-derived exosomal mir-186 inhibits neuroblastoma growth and immune escape mechanisms. *Cancer Res.* **79**, 1151–1164 (2019).
9. X. Wang, Z. Xiang, Y. Liu, C. Huang, Y. Pei, X. Wang, H. Zhi, W. H. Wong, H. Wei, I. O. Ng, P. P. Lee, G. C. Chan, Y. L. Lau, W. Tu, Exosomes derived from Vδ2-T cells control Epstein-Barr virus-associated tumors and induce T cell antitumor immunity. *Sci. Transl. Med.* **12**, eaaz3426 (2020).
10. S. E. Headland, H. R. Jones, L. V. Norling, A. Kim, P. R. Souza, E. Corsiero, C. D. Gil, A. Nerviani, F. Dell'Accio, C. Pitzalis, S. M. Oliani, L. Y. Jan, M. Perretti, Neutrophil-derived microvesicles enter cartilage and protect the joint in inflammatory arthritis. *Sci. Transl. Med.* **7**, 315ra190 (2015).
11. J. Gao, S. Wang, Z. Wang, High yield, scalable and remotely drug-loaded neutrophil-derived extracellular vesicles (EVs) for anti-inflammation therapy. *Biomaterials* **135**, 62–73 (2017).
12. G. H. Nam, Y. Choi, G. B. Kim, S. Kim, S. A. Kim, I. S. Kim, Emerging prospects of exosomes for cancer treatment: from conventional therapy to immunotherapy. *Adv. Mater.* **32**, e2002440 (2020).
13. X. Zhang, H. Zhang, J. Gu, J. Zhang, H. Shi, H. Qian, D. Wang, W. Xu, J. Pan, H. A. Santos, Engineered extracellular vesicles for cancer therapy. *Adv. Mater.* **33**, e2005709 (2021).
14. N. L. Syn, L. Wang, E. K.-H. Chow, C. T. Lim, B. C. Goh, Exosomes in cancer nanomedicine and immunotherapy: prospects and challenges. *Trends Biotechnol.* **35**, 665–676 (2017).
15. O. M. Elsharkasy, J. Z. Nordin, D. W. Hagey, O. G. de Jong, R. M. Schiffelers, S. E. Andaloussi, P. Vader, Extracellular vesicles as drug delivery systems: Why and how? *Adv. Drug Deliv. Rev.* **159**, 332–343 (2020).
16. P. H. L. Tran, D. Xiang, T. T. D. Tran, W. Yin, Y. Zhang, L. Kong, K. Chen, M. Sun, Y. Li, Y. Hou, Y. Zhu, W. Duan, Exosomes and nanoengineering: A match made for precision therapeutics. *Adv. Mater.* **32**, e1904040 (2020).
17. S. C. Jang, O. Y. Kim, C. M. Yoon, D. S. Choi, T. Y. Roh, J. Park, J. Nilsson, J. Lotvall, Y. K. Kim, Y. S. Gho, Bioinspired exosome-mimetic nanovesicles for targeted delivery of chemotherapeutics to malignant tumors. *ACS Nano* **7**, 7698–7710 (2013).
18. T. R. Lunavat, S. C. Jang, L. Nilsson, H. T. Park, G. Repiska, C. Lasser, J. A. Nilsson, Y. S. Gho, J. Lotvall, RNAi delivery by exosome-mimetic nanovesicles—Implications for targeting c-Myc in cancer. *Biomaterials* **102**, 231–238 (2016).
19. Y. W. Choo, M. Kang, H. Y. Kim, J. Han, S. Kang, J. R. Lee, G. J. Jeong, S. P. Kwon, S. Y. Song, S. Go, M. Jung, J. Hong, B. S. Kim, M1 macrophage-derived nanovesicles potentiate the anticancer efficacy of immune checkpoint inhibitors. *ACS Nano* **12**, 8977–8993 (2018).
20. J. R. Lee, B. W. Park, J. Kim, Y. W. Choo, H. Y. Kim, J. K. Yoon, H. Kim, J. W. Hwang, M. Kang, S. P. Kwon, S. Y. Song, I. O. Ko, J. A. Park, K. Ban, T. Hyeon, H. J. Park, B. S. Kim, Nanovesicles derived from iron oxide nanoparticles-incorporated mesenchymal stem cells for cardiac repair. *Sci. Adv.* **6**, eaaz0952 (2020).
21. A. L. Coughlin, D. Xie, Y. Yao, X. Zhan, Q. Chen, H. Hewa-Walpitage, X. Zhang, H. Guo, H. Zhou, J. Lou, J. Wang, Y. S. Li, H. A. Fertig, S. Zhang, Near degeneracy of magnetic phases in two-dimensional chromium telluride with enhanced perpendicular magnetic anisotropy. *ACS Nano* **14**, 15256–15266 (2020).
22. A. Tomitaka, S. Ota, K. Nishimoto, H. Arami, Y. Takemura, M. Nair, Dynamic magnetic characterization and magnetic particle imaging enhancement of magnetic-gold core-shell nanoparticles. *Nanoscale* **11**, 6489–6496 (2019).
23. H. Saari, E. Lazaro-Ibanez, T. Viitala, E. Vuorimaa-Laukkanen, P. Siljander, M. Yliperttula, Microvesicle- and exosome-mediated drug delivery enhances the cytotoxicity of Paclitaxel in autologous prostate cancer cells. *J. Control. Release* **220**, 727–737 (2015).
24. G. B. Kim, G. H. Nam, Y. Hong, J. Woo, Y. Cho, I. C. Kwon, Y. Yang, I. S. Kim, Xenogenization of tumor cells by fusogenic exosomes in tumor microenvironment ignites and propagates antitumor immunity. *Sci. Adv.* **6**, (2020).
25. C. Wen, R. C. Seeger, M. Fabbri, L. Wang, A. S. Wayne, A. Y. Jong, Biological roles and potential applications of immune cell-derived extracellular vesicles. *J. Extracell. Vesicles* **6**, 1400370 (2017).
26. J. Wang, W. Tang, M. Yang, Y. Yin, H. Li, F. Hu, L. Tang, X. Ma, Y. Zhang, Y. Wang, Inflammatory tumor microenvironment responsive neutrophil exosomes-based drug delivery system for targeted glioma therapy. *Biomaterials* **273**, 120784 (2021).
27. D. Zhi, T. Yang, J. Yang, S. Fu, S. Zhang, Targeting strategies for superparamagnetic iron oxide nanoparticles in cancer therapy. *Acta Biomater.* **102**, 13–34 (2020).

28. M. Zhuang, D. Du, L. Pu, H. Song, M. Deng, Q. Long, X. Yin, Y. Wang, L. Rao, SPION-decorated exosome delivered BAY55-9837 targeting the pancreas through magnetism to improve the blood GLC response. *Small* **15**, e1903135 (2019).
29. M. Zhuang, X. Chen, D. Du, J. Shi, M. Deng, Q. Long, X. Yin, Y. Wang, L. Rao, SPION decorated exosome delivery of TNF-α to cancer cell membranes through magnetism. *Nanoscale* **12**, 173–188 (2020).
30. W. Zhang, Z. L. Yu, M. Wu, J. G. Ren, H. F. Xia, G. L. Sa, J. Y. Zhu, D. W. Pang, Y. F. Zhao, G. Chen, Magnetic and folate functionalization enables rapid isolation and enhanced tumor-targeting of cell-derived microvesicles. *ACS Nano* **11**, 277–290 (2017).
31. H. Qi, C. Liu, L. Long, Y. Ren, S. Zhang, X. Chang, X. Qian, H. Jia, J. Zhao, J. Sun, X. Hou, X. Yuan, C. Kang, Blood exosomes endowed with magnetic and targeting properties for cancer therapy. *ACS Nano* **10**, 3323–3333 (2016).
32. F. M. Kievit, Z. R. Stephen, O. Veiseh, H. Arami, T. Wang, V. P. Lai, J. O. Park, R. G. Ellenbogen, M. L. Disis, M. Zhang, Targeting of primary breast cancers and metastases in a transgenic mouse model using rationally designed multifunctional SPIONs. *ACS Nano* **6**, 2591–2601 (2012).
33. Y. Tian, S. Li, J. Song, T. Ji, M. Zhu, G. J. Anderson, J. Wei, G. Nie, A doxorubicin delivery platform using engineered natural membrane vesicle exosomes for targeted tumor therapy. *Biomaterials* **35**, 2383–2390 (2014).
34. S. Li, Y. Wu, F. Ding, J. Yang, J. Li, X. Gao, C. Zhang, J. Feng, Engineering macrophage-derived exosomes for targeted chemotherapy of triple-negative breast cancer. *Nanoscale* **12**, 10854–10862 (2020).
35. M. Fusciello, F. Fontana, S. Tähtinen, C. Capasso, S. Feola, B. Martins, J. Chiaro, K. Peltonen, L. Ylösmäki, E. Ylösmäki, F. Hamdan, O. K. Kari, J. Ndika, H. Alenius, A. Urtti, J. T. Hirvonen, H. A. Santos, V. Cerullo, Artificially cloaked viral nanovaccine for cancer immunotherapy. *Nat. Commun.* **10**, 5747 (2019).
36. H. Zhang, W. Cui, X. Qu, H. Wu, L. Qu, X. Zhang, E. Mäkilä, J. Salonen, Y. Zhu, Z. Yang, D. Chen, H. A. Santos, M. Hai, D. A. Weitz, Photothermal-responsive nanosized hybrid polymersome as versatile therapeutics codelivery nanovehicle for effective tumor suppression. *Proc. Natl. Acad. Sci. U.S.A.* **116**, 7744–7749 (2019).
37. F. Fontana, M. Fusciello, C. Groeneveldt, C. Capasso, J. Chiaro, S. Feola, Z. Liu, E. M. Mäkilä, J. J. Salonen, J. T. Hirvonen, V. Cerullo, H. A. Santos, Biohybrid vaccines for improved treatment of aggressive melanoma with checkpoint inhibitor. *ACS Nano* **13**, 6477–6490 (2019).
38. T. Yong, X. Zhang, N. Bie, H. Zhang, X. Zhang, F. Li, A. Hakeem, J. Hu, L. Gan, H. A. Santos, X. Yang, Tumor exosome-based nanoparticles are efficient drug carriers for chemotherapy. *Nat. Commun.* **10**, 3838 (2019).
39. D. Chu, X. Dong, X. Shi, C. Zhang, Z. Wang, Neutrophil-based drug delivery systems. *Adv. Mater.* **30**, e1706245 (2018).
40. J. Che, A. Najer, A. K. Blakney, P. F. McKay, M. Bellahcene, C. W. Winter, A. Sintou, J. Tang, T. J. Keane, M. D. Schneider, R. J. Shattock, S. Sattler, M. M. Stevens, Neutrophils enable local and non-invasive liposome delivery to inflamed skeletal muscle and ischemic heart. *Adv. Mater.* **32**, e2003598 (2020).
41. T. Kang, Q. Zhu, D. Wei, J. Feng, J. Yao, T. Jiang, Q. Song, X. Wei, H. Chen, X. Gao, J. Chen, Nanoparticles coated with neutrophil membranes can effectively treat cancer metastasis. *ACS Nano* **11**, 1397–1411 (2017).
42. J. Xue, Z. Zhao, L. Zhang, L. Xue, S. Shen, Y. Wen, Z. Wei, L. Wang, L. Kong, H. Sun, Q. Ping, R. Mo, C. Zhang, Neutrophil-mediated anticancer drug delivery for suppression of postoperative malignant glioma recurrence. *Nat. Nanotechnol.* **12**, 692–700 (2017).

Acknowledgments: We thank the members of the Zhang laboratory for helpful discussion and paper preparation. **Funding:** This work was supported by the National Natural Science Foundation of China (81972310, 22078132, and 21822807), Distinguished Young Scholar Project of Jiangsu Province (BK20200043), Major Natural Science Research Project for Universities in Jiangsu Province (18KJA320001), Key Laboratory of Molecular Diagnostics and Precision Medicine for Surgical Oncology in Gansu Province (2019GSZDSYS01 and 2019GSZDSYS02), Priority Academic Program Development of Jiangsu Higher Education Institutions (PAPD), Distinguished Clinical Investigator Grant of Jiangsu Province (JSTP201701), and Jiangsu Provincial Key Research and Development Programme (grant no. BE2018690). H.A.S. acknowledges financial support from the Sigrid Jusélius Foundation and the Academy of Finland (decision nos. 317042 and 331151). **Author contributions:** X.Z. conceived the project and supervised the research. J.Z., C.J., and H.Z. performed all experimental aspects of the project, analyzed and interpreted data, and prepared the manuscript. H.S., F.M., H.Q., W.X., D.W., J.P., X.F., H.Z., H.A.S., and X.Z. provided funds and other resources, as well as assisted with data interpretation and preparation of the manuscript. **Competing interests:** The authors declare that they have no competing interests. **Data and materials availability:** All data needed to evaluate the conclusions in the paper are present in the paper and/or the Supplementary Materials.

Submitted 3 June 2021
Accepted 19 November 2021
Published 12 January 2022
10.1126/sciadv.abj8207

ScienceAdvances

Engineered neutrophil-derived exosome-like vesicles for targeted cancer therapy

Jiahui ZhangCheng JiHongbo ZhangHui ShiFei MaoHui QianWenrong XuDongqing WangJianming PanXinjian FangHélder A. SantosXu Zhang

Sci. Adv., 8 (2), eabj8207. • DOI: 10.1126/sciadv.abj8207

Science Advances (ISSN) is published by the American Association for the Advancement of Science. 1200 New York Avenue NW, Washington, DC 20005. The title *Science Advances* is a registered trademark of AAAS.